

Fullerene Nanoparticles Selectively Enter Oxidation-Damaged Cerebral Microvessel Endothelial Cells and Inhibit JNK-Related Apoptosis

Fang Lao,^{*,†} Long Chen,^{*,†} Wei Li,^{§,†} Cuicui Ge,^{§,†} Ying Qu,^{*,†} Quanmei Sun,^{*,†} Yuliang Zhao,^{§,†} Dong Han,^{*,†,*} and Chunying Chen^{*,†,*}

[†]CAS Key Lab for Biological Effects of Nanomaterials and Nanosafety (NCNST-IHEP), [‡]National Center for Nanoscience and Technology (NCNST), Beijing 100190, China, and [§]Institute of High Energy Physics (IHEP), Chinese Academy of Sciences, Beijing 100049, China

ABSTRACT There is a dearth in fundamental cellular-level understanding of how nanoparticles interact with the cells of the blood brain barrier (BBB), particularly under the oxidative environment. The apoptosis of cerebral microvessel endothelial cells (CMECs) induced by oxidative stress injury plays a key role in the dysfunction of BBB. By use of CMECs as an *in vitro* BBB model, we show for the first time that C₆₀(C(COOH)₂)₂ nanoparticles can selectively enter oxidized CMECs rather than normal cells, and maintain CMECs integrity by attenuating H₂O₂-induced F-actin depolymerization *via* the observation of several state-of-the-art microscopic techniques. Additionally, we have found that C₆₀(C(COOH)₂)₂ nanoparticles greatly inhibit the apoptosis of CMECs induced by H₂O₂, which is related to their modulation of the JNK pathway. C₆₀(C(COOH)₂)₂ nanoparticles can regulate several downstream signaling events related to the JNK pathway, including reduction of JNK phosphorylation, activation of activator protein 1 (AP-1) and caspase-3, and inhibition of polyADP-ribose polymerase (PARP) cleavage and mitochondrial cytochrome *c* release. Our results indicate that C₆₀(C(COOH)₂)₂ nanoparticles possess a novel ability of selectively entering oxidation-damaged cerebral endothelial cells rather than normal endothelial cells and then protecting them from apoptosis.

KEYWORDS: C₆₀(C(COOH)₂)₂ · microvessel endothelial cells · oxidative injury · apoptosis · JNK pathway

In the past decade, nanoparticles have become an important class of novel materials with several properties that make them very attractive for drug development in the biomedical field.¹ Nanotechnology has been applied to diverse medical uses such as biomarkers discovery, molecular diagnostics, and drug delivery, which could be applicable to management of cancer,² inflammation, neurodegenerative disease³ and cardiovascular disorder.⁴

The development of nanotechnology based-drugs also enables applications in antioxidant defense. Evidence has accumulated during the past two decades showing that reactive oxygen species (ROS) are involved in many neurologic disorders and brain dysfunctions.^{5,6} Harmful effects of ROS arise when there

is overproduction of free radicals to the extent that antioxidative enzymatic systems are overloaded. Because of the high oxygen metabolism of the blood brain barrier (BBB), the mitochondrial content in cerebral microvessel endothelial cells (CMECs) is higher than in peripheral endothelial cells.⁷ As a result, the concentration of ROS, products of cellular oxygen metabolism, is also relatively higher. In view of this, CMECs are particularly vulnerable to oxidative damage and suffer from ROS-induced dysfunction.⁸ Injury may occur easily in the BBB, resulting in impaired selectivity and decreased function, which is involved in a series of downstream disorders and finally causes central nervous system (CNS) microenvironment exposure and neural injury. It is therefore necessary to identify antiapoptotic agents or free radical scavengers to counteract the detrimental effects of ROS on CMECs.

Many recognized antioxidants, including natural nutrients like carotenoids, vitamin C, and biochemical components such as vasoactive endocannabinoid, 2-arachidonoyl glycerol, and uric acid, have been shown to have potent efficiency in diminishing the cumulative effects of exogenous oxidative damage.^{9–11} In addition to these traditional antioxidants, some studies indicate that nanoparticles, also present powerful free-radical scavenging capacity, making them good candidates as potential antioxidants.¹² Furthermore, compared with traditional antioxidants, nanoparticles possess higher physical stability when in contact with biological fluids and permit con-

*Address correspondence to chenchy@nanocr.cn, dhan@nanocr.cn.

Received for review August 2, 2009 and accepted October 7, 2009.

Published online October 19, 2009. 10.1021/nn900912n CCC: \$40.75

© 2009 American Chemical Society

trolled and sustained drug release,¹³ thus extending their applications to the treatment of the effects of accumulated oxidation stimulus and continuous damage.

Under normal physiological conditions, nanoparticles with antioxidative efficacy also are appropriate candidates for maintaining the ROS formation/reduction balance of CMECs, because the higher ROS levels produced by mitochondria in CMECs mean that they are exposed to continuous oxidative stimulation throughout the entire life cycle of the cell. Under pathological conditions, the production of ROS, resulting in potential oxidative damage, is a cumulative process. Thus, investigation of the potential of nanoparticles for therapy in oxidative-induced BBB dysfunctions is receiving more and more attention due to their efficacy and stable properties.

However, although some nanoparticles have been demonstrated to protect the brain for oxidation damage,^{14,15} very little is known about the response of CMECs to the antioxidative nanoparticles, and there are no investigations for the intracellular behavior of nanoparticles under physiological and pathological conditions, or of the molecular mechanism underlying their effects. Therefore, the main aim of this study is to observe the behavior and effect of nanoparticle with antioxidative capacity on CMECs, and investigate whether nanoparticles are beneficial in counteracting the harmful effects of ROS in brain microvessels. We used bimaleic acid fullerene derivative $C_{60}(C(COOH)_2)_2$ in this study and designed a series of experiments to investigate the effects of $C_{60}(C(COOH)_2)_2$ on CMECs under both physiological and oxidative injury conditions.

$C_{60}(C(COOH)_2)_2$ belongs to a group of antioxidant nanoparticles named hydrophilic fullerene derivatives, and have been well studied over the past 10 years for their high reactivity with oxygen free radicals.^{14,15} Dugan *et al.* (1997) have shown that a similar derivative $C_{60}(C(COOH)_2)_3$ (C3) is an effective neuroprotective antioxidant¹⁵ that can efficiently prevent dopaminergic neuron apoptosis *in vitro* and protect cerebellar granule cells from apoptosis. In addition, reports have also indicated that C3 can block iron-induced lipid peroxidation *in vivo*,¹⁶ and reduce basal mitochondrial production of superoxide in cortical astrocytes.¹⁷ However, although several reports have shown that maleic acid fullerene derivatives have excellent neural protective efficacy in a broad spectrum of neurodisorders,^{15,18} the basis of this efficacy, particularly whether nanoparticles translocate into the cell under opposing physiological conditions (normal/oxidative), the correlation between translocation of nanoparticles into the cell and cell oxidative status, and the molecular mechanism underlying these protective effects, are still controversial. Therefore, in this study, we have focused on elucidating the cellular and molecular events that occur when $C_{60}(C(COOH)_2)_2$ nanoparticles encounter brain micro-

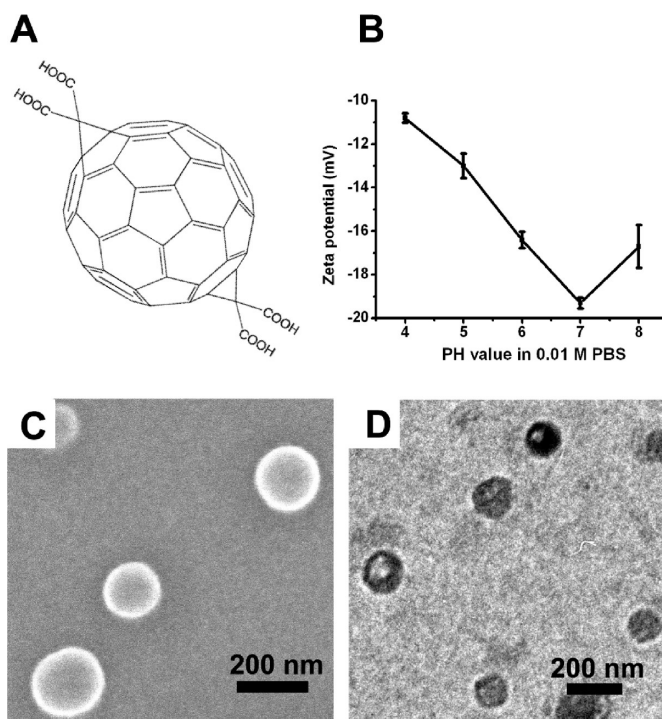


Figure 1. Characterization of fullerene derivative $C_{60}(C(COOH)_2)_2$. Structures (A) and ζ potential (B) are shown. SEM (C) and TEM (D) images of $C_{60}(C(COOH)_2)_2$ aggregations; 50 μ M fullerene derivative $C_{60}(C(COOH)_2)_2$ nanoparticles were prepared in 0.01 M PBS before observation. The average size of $C_{60}(C(COOH)_2)_2$ aggregation is about 150 nm.

vessel endothelial cells and supplying a reasonable explanation for their protective effect.

RESULTS AND DISCUSSION

Preparation and Characterization of $C_{60}(C(COOH)_2)_2$

Nanoparticles. Initially, highly purified C_{60} -fullerene derivative $C_{60}(C(COOH)_2)_2$ was synthesized and characterized as described previously.^{19–21} Because of the regiochemistry of polyadducts,^{19,20} we further separated the products with HPLC, characterized them by TOF-MS, and finally the *trans*-2 isomer (Figure 1A) was chosen to study the biological effects in the following experiments.

Zeta (ζ) potential in 0.01 M phosphate buffered saline (PBS) was performed with Nano ZS 90 (Malvern). The ζ potential displayed an interesting trend: the absolute ζ potentials of $C_{60}(C(COOH)_2)_2$ increased with the increased pH value. The change of ζ potential with pH (Figure 1B) indicates that $C_{60}(C(COOH)_2)_2$ particles are most stable under physiological pH (7.0) and get unstable in lower pH condition. This feature may promote the use in cellular system owing to intercellular endosomes with lower pH, which may disaggregate the $C_{60}(C(COOH)_2)_2$ nanoparticles into smaller fractions. Although the diameter of an isolated $C_{60}(C(COOH)_2)_2$ molecule is about 0.7 nm, it readily forms aggregations of about 150 nm at the concentration of 50 μ M, which were characterized with scanning electron microscopy (SEM, Hitachi S-4800, Japan) (Figure 1C) and transmis-

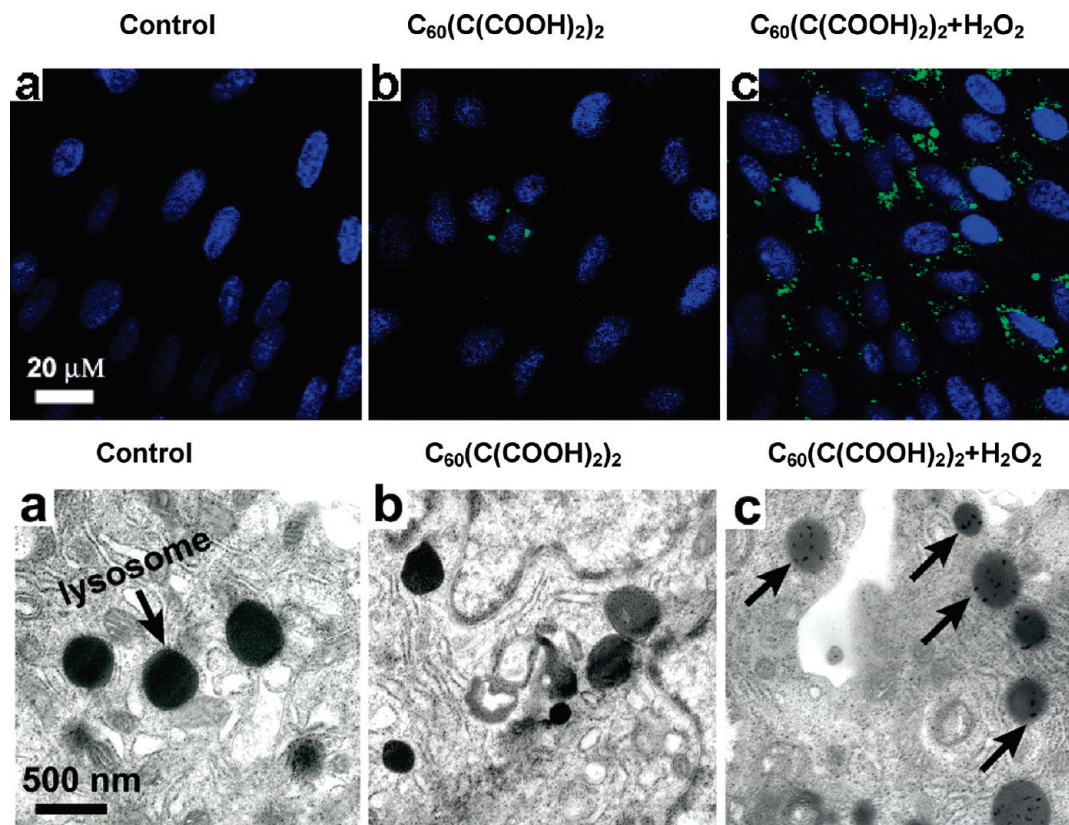


Figure 2. Oxidative stimulation allowed more $C_{60}(C(COOH)_2)_2$ nanoparticles to enter into the cell. Normal CMECs (A-a), FITC- $C_{60}(C(COOH)_2)_2$ treated CMECs (A-b), and FITC- $C_{60}(C(COOH)_2)_2 + H_2O_2$ incubated CMECs (A-c) were observed with confocal microscopy. The images showed that the fluorescence of FITC- $C_{60}(C(COOH)_2)_2$ increased significantly after H_2O_2 stimulation (A-c). The ultrastructural observations with TEM (B) confirmed the results. Condensed $C_{60}(C(COOH)_2)_2$ nanoparticle aggregates were observed in endosome-like vesicles (arrows) after oxidative stimulation (B-c), whereas normal controls (B-a) and cells incubated with $C_{60}(C(COOH)_2)_2$ (B-b) showed homogeneous endosome staining.

sion electronic microscopy (TEM, FEG-TF20) (Figure 1D). The size of aggregation depends on the fullerene concentration. As the results from solid-state SEM and TEM imaging do not necessarily translate to the solution state, we also determined the size distribution of $C_{60}(C(COOH)_2)_2$ in aqueous solution by using dynamic light scattering (DLS) (Figure S1 of Supporting Information). DLS data indicate the average size is 167.5 nm, which is similar to values obtained by TEM and SEM.

Oxidative Stimulation Increased Translocation of Nanoparticles into the Cells. Subsequently, to determine whether nanoparticles can be translocated into the cell, we labeled $C_{60}(C(COOH)_2)_2$ with the fluorescent dye FITC as described.²⁰ This enabled direct observation of the cellular distribution of $C_{60}(C(COOH)_2)_2$ using confocal microscopy. Intact CMECs were used to normalize the fluorescent background (Figure 2A-a) and cell nuclei were detected by Hoechst 33342 (Sigma-Aldrich Co.). Unexpectedly, the intracellular intensity of fluorescent nanoparticles after H_2O_2 exposure (Figure 2A-c) was found to be significantly enhanced compared to CMECs not treated with oxidant incubation (Figure 2A-b). The results suggest that the oxidant stimulation distinctly facilitated the uptake of nanoparticles by CMECs. Strong fluorescent spots were localized at the cell

plasma (Figure 2A-c), and colocalization experiments by different organelle specific fluorescent probes such as Lyso Tracker Red or Mito Tracker Red further demonstrated that the particles accumulated in lysosomes instead of in mitochondria. (Figure S2 of Supporting Information).

The results were further confirmed by TEM observations. $C_{60}(C(COOH)_2)_2$ aggregations were clearly localized in lysosome structures in H_2O_2 -treated CMECs (Figure 2B-c, black arrow). However, there was no obvious accumulation of particles in untreated samples (Figure 2B-a,b) and lysosome staining was homogeneous.

Oxidative Stimulation Enhanced Existence of Nanoparticles on CMECs Membrane. To explore the reason why more nanoparticles were translocated into the cell after H_2O_2 stimulation, and to further compare the cellular uptake of nanoparticles under normal condition and after oxidation damage, a biological atom force microscopy (AFM) is used (Agilent Co). Since substantial evidence indicates that treatment of cells with oxidants overload can result in the production of lipid peroxides,²² affect the function of membrane proteins,²³ and modify cell membrane structure,²⁴ in this study AFM is employed to “palpate” the membrane precisely at the nanoscale level and image the morphological response of the

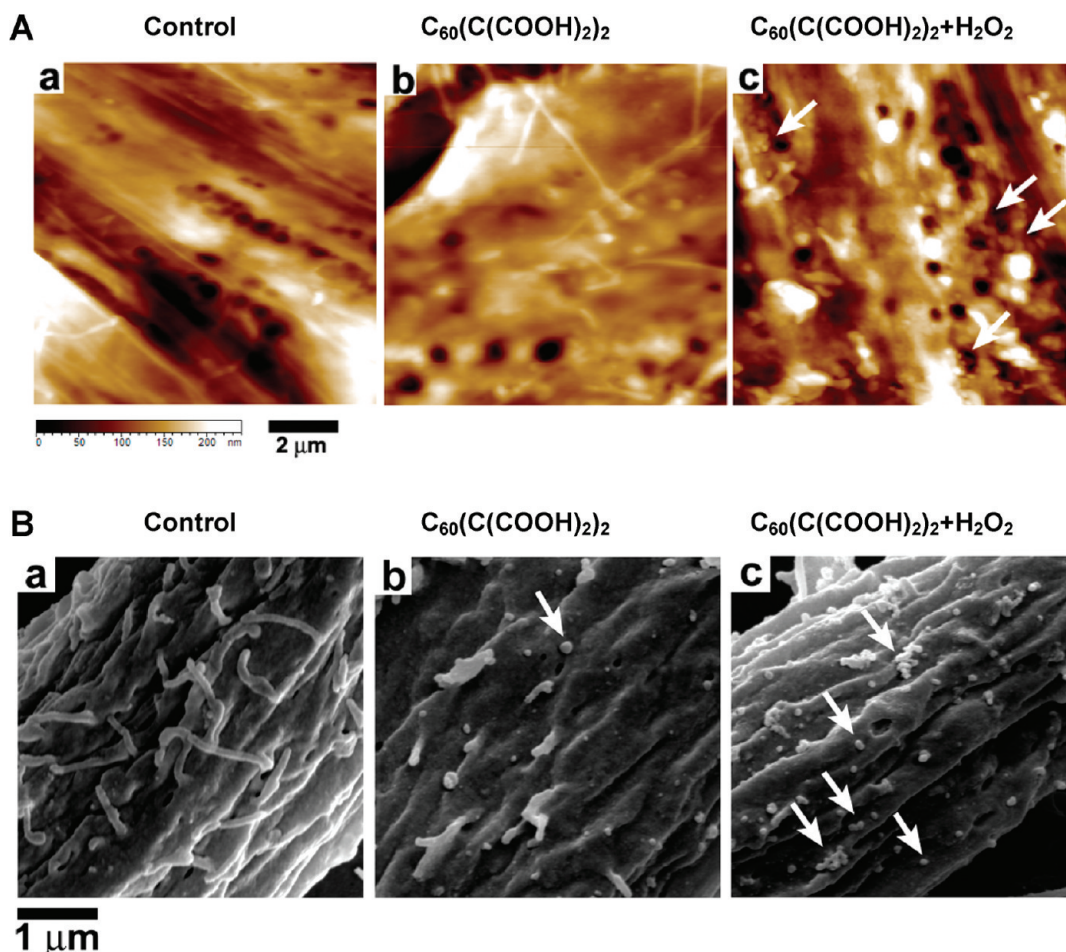


Figure 3. Oxidative stimulation greatly enhanced nanoparticles adherence to the CMECs membrane. Normal cells (A-a and B-a), $C_{60}(C(COOH)_2)_2$ (50 μM) treated cells (A-b and B-b), and $C_{60}(C(COOH)_2)_2$ (50 μM) + H_2O_2 (300 μM) incubated cells (A-c and B-c) were observed with AFM (A) and ESEM (B). More highlighted spots (arrows, A-c and B-c) appeared on plasma membranes of H_2O_2 -stimulated cells than controls (A-a, B-a, and A-b, B-b). The images of AFM showed that some $C_{60}(C(COOH)_2)_2$ were located in the pore-structure formation on the CMECs membrane (A-c).

membrane under oxidative damage or nanoparticle stimulation. Cells treated in the absence of H_2O_2 or without $C_{60}(C(COOH)_2)_2$ nanoparticles were fixed with 2.5% (v/v) glutaraldehyde and prepared for AFM as described.²⁵ Surface areas of 10 μm were randomly selected for scanning by the instrument, and at least four areas were scanned for each treatment. The images obtained show that there was a variable number of particles on the surface of CMECs after $C_{60}(C(COOH)_2)_2$ incubation. Interestingly, $C_{60}(C(COOH)_2)_2$ aggregations administered after H_2O_2 treatment gave rise to highlighted spots (nanoparticles, white arrows) on the cell membrane (Figure 3A-c); in some areas these particles were observed to pit into the fenestra structure, indicating specific interaction of functional nanoparticles with the oxidation-damaged cell membrane. The number of spots on cells that were incubated with fullerene particles alone (Figure 3A-b) was lower than that for oxidation-damaged samples, close to that for the controls (Figure 3A-a).

We confirmed the results by using an environmental scanning electronic microscopy (ESEM) (Quanta 200

FEG, FEI Co.). The potent advantage to using ESEM is that it is not necessary to make a nonconductive sample conductive. Cell samples do not need to be coated with gold–palladium, and thus their original characteristics may be preserved for observation. By using this instrument, we obtained similar results. More spots were observed in oxidation-damaged samples (Figure 3B-c, white arrows) compared to the controls (Figure 3B-b). Fullerene aggregations were bound primarily to the cell membrane and some were observed to be nonspecifically embedded into the membrane.

Additionally, CMECs are characterized by the presence of tight junctions (TJs), the lack of fenestrations, and a paucity of pinocytotic vesicles, which is distinct from other cells. The experimental results indicate that the FITC- $C_{60}(C(COOH)_2)_2$ hardly enters the rCMECs under normal condition. In contrast, FITC- $C_{60}(C(COOH)_2)_2$ can easily enter many other cell types without any stimulation in our previous publication.²⁰ We have explored the processes of $C_{60}(C(COOH)_2)_2$ across cellular membranes and their intracellular translocation in normal 3T3 L1 and RH-35 living cells.

The relationship between oxidative stimulation and increasing amounts of inter/extra cellular particles requires further investigation. Several investigators expatiate that cell membrane has a total negative electric charge; oxidative stress to cell membrane may lead to a significant decrease of cell surface charge.^{26,27} The intriguing explanation to our results may be that $C_{60}(C(COOH)_2)_2$ nanoparticles with negative charge are repulsed by CMECs under normal physiological situation. The decrease of negative surface charge after exogenous ROS stimulation may facilitate the adherence of $C_{60}(C(COOH)_2)_2$ to the cell membrane, improving the opportunity for nanoparticle translocation. Other data also have demonstrated that oxidative stress to sialic acid that bears a negative charge may play a role in the aggregation of erythrocytes, increasing the adhesiveness to endothelial cells contributing to the development of various pathologies.^{28,29} In addition, a loss in negative charge of CMECs may be paralleled by changes in cell structure and function, which result in a change of CMECs hypersensitivity to nanoparticles. Evidence supporting this hypothesis is under investigation in our lab.

Translocated $C_{60}(C(COOH)_2)_2$ Nanoparticles Can Protect CMECs from H_2O_2 -Induced Damage. Another finding revealed in this study is that the administration of $C_{60}(C(COOH)_2)_2$ in CMECs after oxidative assault markedly reduced the number of apoptotic cells. CMECs were stimulated with 300 μM H_2O_2 for 2 h and incubated with $C_{60}(C(COOH)_2)_2$ nanoparticles at five concentrations from 25 to 200 μM for 24 h, then cell viability was determined using the CCK-8 assay (Dojindo Laboratories, Co.). Cell counts show that $C_{60}(C(COOH)_2)_2$ reduced H_2O_2 injury in a dose-dependent fashion (Figure 4A), and the effective dose 50% (ED_{50}) of nanoparticles is 55.2 ± 2.31 μM . To show whether $C_{60}(C(COOH)_2)_2$ neutralizes oxidative toxicity by regulating apoptosis, fluorescence double staining with Annexin V-FITC and PI was used. A significant signal of protection was detected by flow cytometry, and the percentage of apoptotic cells treated with 50 or 100 μM $C_{60}(C(COOH)_2)_2$ for 24 h was 12.3% (Figure 4B-c) and 7.1% (Figure 4B-d), respectively, significantly less than the untreated group (49.4%) (Figure 4B-b), but higher than the control (4.2%) (Figure 4B-a). These data show that $C_{60}(C(COOH)_2)_2$ nanoparticles have a potent protective effect against oxidative damage, concurring with previous data demonstrating the ability of fullerene derivatives to inhibit ROS-induced cortical neuron apoptosis.¹⁵

More interestingly, images of TEM in further experiments show that the shape of mitochondria in controls and $C_{60}(C(COOH)_2)_2$ treated group was normal (Figure 4C-a,b). After exposure to H_2O_2 , the morphology of CMECs was typical of apoptosis, characterized by mitochondrial swelling (Figure 4C-c, black arrows). However, apoptosis induced by H_2O_2 was markedly attenuated by the addition of

$C_{60}(C(COOH)_2)_2$ nanoparticles (100 μM) (Figure 4C-d). Therefore, these results provide strong histological evidence demonstrating that $C_{60}(C(COOH)_2)_2$ had protective effects when CMECs were exposed to oxidative injury. Previous antioxidant studies demonstrated that $C_{60}(C(COOH)_2)_n$ can reduce basal mitochondrial production of superoxide radical anions in cortical astrocytes and neurons,¹⁸ which may partly explain the phenomenon in our model that $C_{60}(C(COOH)_2)_2$ effectively maintained normal morphology of mitochondria in oxidative environments. It should be noted that the explanation for the correlation of cell survival with increased quantities of $C_{60}(C(COOH)_2)_2$ translocation is still controversial, and evidence for an underlying mechanism for oxidative stress modulation also requires further investigation.

Although under physiological situation much less $C_{60}(C(COOH)_2)_2$ was observed in CMECs, the cytotoxicity of $C_{60}(C(COOH)_2)_2$ still needs to be estimated. Our results show that in a pharmacological range, $C_{60}(C(COOH)_2)_2$ had no impact on cell growth and basic function of normal CMECs, indicating that it has good biocompatibility under normal physiological conditions (Figure S3 of Supporting Information).

$C_{60}(C(COOH)_2)_2$ Stabilized CMECs Integrity by Attenuating H_2O_2 -Induced F-Actin Depolymerization. To address how $C_{60}(C(COOH)_2)_2$ are beneficial for endothelial function other than by their antiapoptotic effects, we investigated the mechanism of $C_{60}(C(COOH)_2)_2$ action on CMECs permeability caused by changes in F-actin density and arrangement. The actin cytoskeleton plays a critical role in the physiological maintenance of the BBB.³⁰ High levels of H_2O_2 exposure result in intercellular gap formation decrease in F-actin density and capillary endothelial cell apoptosis. To investigate whether $C_{60}(C(COOH)_2)_2$ nanoparticles cause changes in the structural arrangement of F-actin under oxidative pathological assault, we examined actin filaments with rhodamine-labeled phalloidin (Molecular Probes, USA). Results show that, $C_{60}(C(COOH)_2)_2$ alone did not change the arrangement and expression level of F-actin (Figure 5b), but significant losses of actin bundles were detected in cells treated with H_2O_2 (Figure 5c). Treatment of CMECs with 100 μM $C_{60}(C(COOH)_2)_2$ potently inhibited H_2O_2 -induced cytoplasm F-actin depolymerization (Figure 5d), with staining at a level close to that of the controls (Figure 5a). As the intercellular gap and degree of permeability are regulated by actin cytoskeletal tension, our results strongly indicate that $C_{60}(C(COOH)_2)_2$ nanoparticles stabilized the integrity of the BBB and maintained its permeability under pathological reoxygenation conditions.

Effects of $C_{60}(C(COOH)_2)_2$ Nanoparticles on ROS and JNK Signaling Events. After observing the protective effect of $C_{60}(C(COOH)_2)_2$ nanoparticles on oxidative assault, we

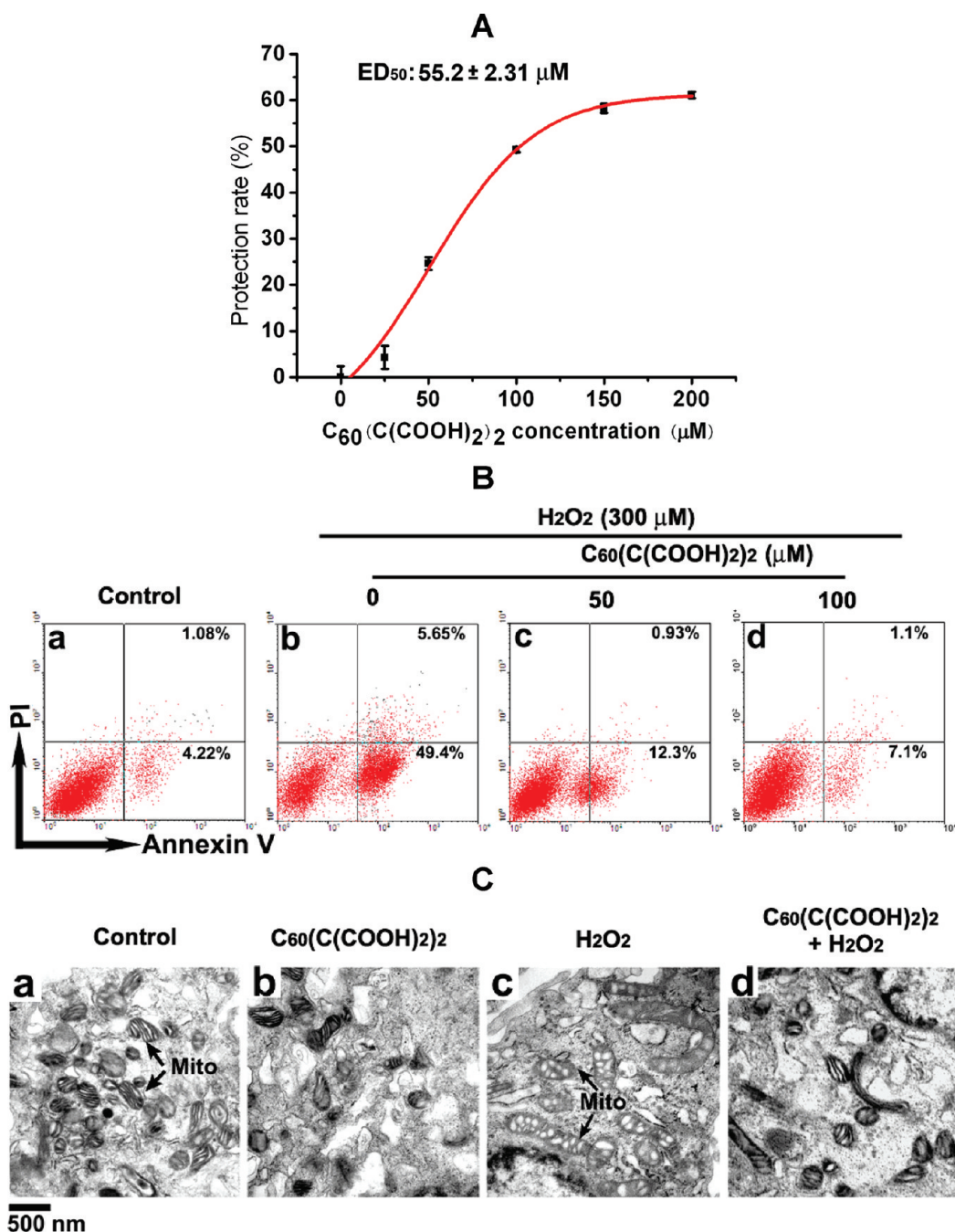


Figure 4. Dose-dependent effects of C₆₀(C(COOH)₂)₂ nanoparticles attenuate H₂O₂-induced death and apoptotic CMECs. (A) Cell viability of CMECs was determined and the ED₅₀ was 55.2 ± 2.31 μM. Data are expressed as means ± SEM; *P* < 0.05. (B) CMECs exposed to H₂O₂ were treated with nanoparticles and were assessed further by Annexin V/PI apoptosis test. Cells were not treated with H₂O₂ (a). Cells exposed to H₂O₂ were treated by C₆₀(C(COOH)₂)₂ nanoparticles at different concentrations of 0 μM (b), 50 μM (c), and 100 μM (d). (C) TEM photographs of normal control (a), C₆₀(C(COOH)₂)₂ (100 μM) treated sample (b), H₂O₂ (300 μM) treated sample (c), and nanoparticles (100 μM) + H₂O₂ (300 μM) (d). Black arrows in H₂O₂-treated cells indicate swelling mitochondria in apoptotic cells.

investigated its mechanism. Reviewing previous publications, we found that fullerene derivative nanoparticles are among the most widely studied nanoparticles with antioxidative properties and have been shown to be involved in protecting a number of cell culture and animal models from oxidation related diseases.³¹ C3 has been found to act as an SOD mimic in neurodegenerative disorders. From the point of view of their ROS scav-

enging, we treated CMECs with DCFH-DA, a fluorescent indicator for ROS, to observe the changes in ROS using confocal microscopy (Figure 6A) and flow cytometry (Figure 6B). Our results showed the sudden increase in ROS induced by H₂O₂ (Figure 6A,B-b) was markedly reduced by C₆₀(C(COOH)₂)₂ nanoparticles in a dose-dependent manner (50, 100 μM) (Figure 6A,B-c,d) compared to controls (Figure 6A,B-a). Our findings in-

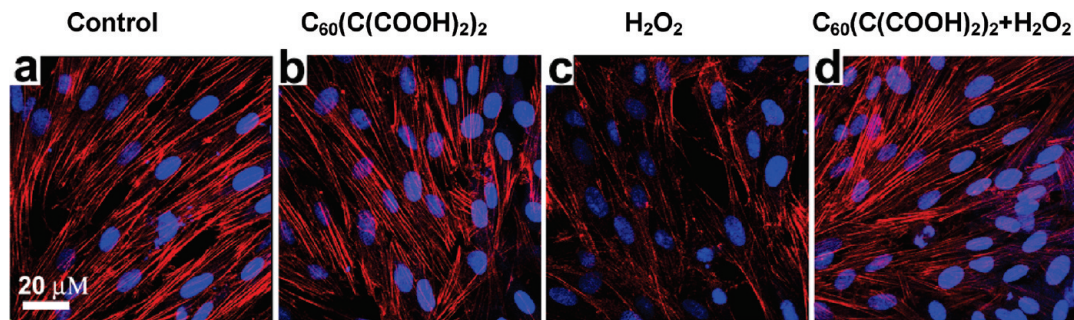


Figure 5. Confocal images of CMECs cytoskeleton. CMECs F-actin alignment and density was stained with rhodamine–phalloidin and recorded by confocal microscopy. Regular and clear filaments were observed in (a) untreated controls, and (b) 100 μM $\text{C}_{60}(\text{COOH})_2$ treated cells, but sparse, dispersed staining was detected in (c) H_2O_2 -exposed cells. In contrast, (d) cells exposed to H_2O_2 and $\text{C}_{60}(\text{COOH})_2$ (100 μM) exhibited a significantly better pattern of cytoskeleton staining.

deed demonstrate that the sudden increase in ROS induced by oxidative stimulation can be normalized by administration of $\text{C}_{60}(\text{COOH})_2$.

Nevertheless, the exact molecular mechanism by which this protection occurs has still to be elucidated. It is known that mitogen-activated protein kinase (MAPK) cascades are stress-sensitive kinases that are likely to be involved in oxidative stress activation and implicated in some forms of apoptotic cell death.³² H_2O_2 is known to be a signaling molecule that can activate MAPK signal transduction pathways, and may modulate cell death in endothelial cells.^{33,34} A number of literatures have shown that activation of c-Jun NH2-

terminal protein kinase (JNK, belongs to MAPK cascades), following oxidative stress, induces apoptosis *via* activation of c-Jun,³⁵ a component of activator protein-1 (AP-1). Therefore, we examined whether nanoparticles protect cells from cellular stress-induced death by interfering with the MAPK pathway. We investigated the expression of extracellular signal-regulated kinase (ERK, components of MAPK cascades), JNK, and phosphorylation of c-Jun. CMECs stimulation with 300 μM H_2O_2 were treated in the presence or absence of 50 and 100 μM $\text{C}_{60}(\text{COOH})_2$; the expression of particular proteins was assessed by Western-blotting using phospho-specific antibodies (Millipore Co.). Western

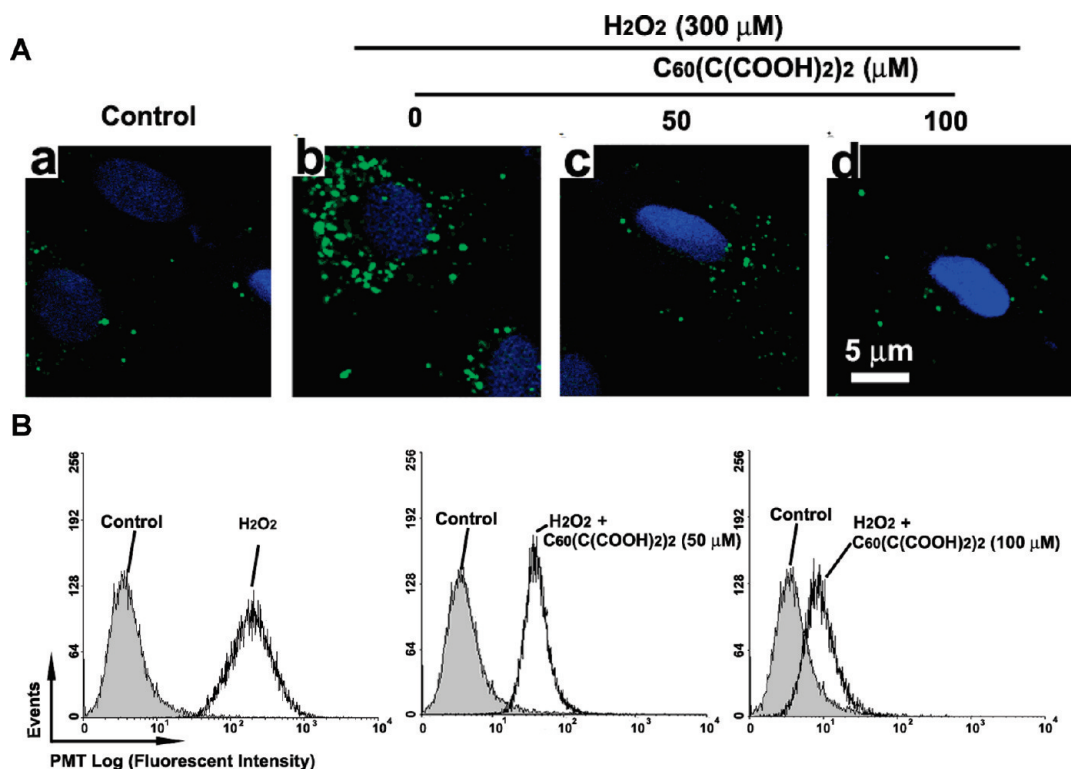


Figure 6. Total intercellular ROS was detected using DCFH-DA followed by confocal microscopy (A) and flow cytometry (B). H_2O_2 -induced formation of ROS and the effects of treatment with $\text{C}_{60}(\text{COOH})_2$ nanoparticles were detected. (A) Confocal image of living cells loaded with DCFH-DA are shown: (a) untreated controls, (b) H_2O_2 (300 μM) treated cells, and (c and d) $\text{C}_{60}(\text{COOH})_2$ nanoparticle (50 and 100 μM) treated cells. Fluorescence was normalized to the control (no H_2O_2) for each sample. Effects of H_2O_2 on intracellular ROS were inhibited by $\text{C}_{60}(\text{COOH})_2$ nanoparticle treatment. (B) Flow cytometry data that are consistent with confocal images are shown for their respective samples (a–c).

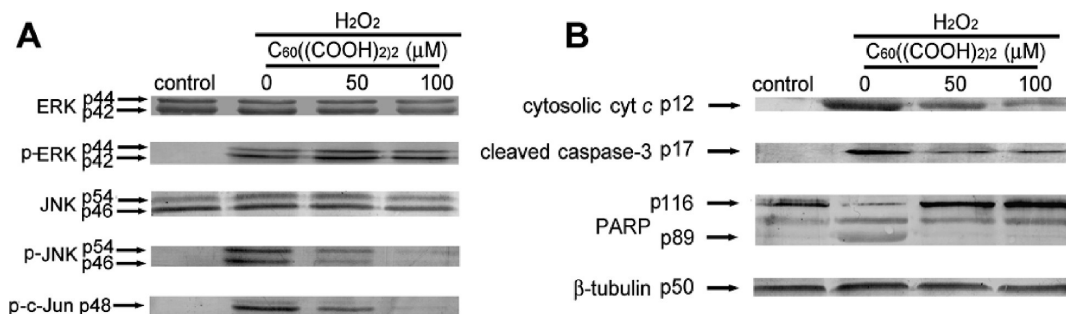


Figure 7. Effects of $C_{60}(C(COOH)_2)_2$ nanoparticles on the MAPK apoptotic pathway. Oxidation CMECs were incubated with $C_{60}(C(COOH)_2)_2$ at the indicated dose. Protein expressions were assessed by Western blotting. (A) $C_{60}(C(COOH)_2)_2$ significantly decreased phosphor-JNK (p-JNK) and phosphor-c-Jun (p-c-Jun), but not phosphor-ERK (p-ERK). Total protein (JNK and ERK) expression was unaltered. (B) Effect of $C_{60}(C(COOH)_2)_2$ nanoparticles on cytosolic cyt c, cleaved caspase-3, and PARP. The inhibitory effects of $C_{60}(C(COOH)_2)_2$ nanoparticles on mitochondrial cyt c release and caspase-3 activation are consistent with effects on JNK phosphorylation. β -Tubulin was used to normalize the quantity of the protein on the blot.

blotting was performed using a previously described method with some modifications.³⁶ As shown in Figure 7A, stimulation with H_2O_2 significantly increased ERK and JNK phosphorylation in CMECs. However, treatment with $C_{60}(C(COOH)_2)_2$ nanoparticles significantly attenuates H_2O_2 -induced JNK phosphorylation, whereas they have little impact on ERK activation.

When we investigated the effect of $C_{60}(C(COOH)_2)_2$ nanoparticles on the activity of the JNK target substrate c-Jun, the expression of phosphorylated c-Jun decreased in $C_{60}(C(COOH)_2)_2$ treated cells, compared with H_2O_2 -treated cells. In CMECs exposed to higher doses (100 μM) of nanoparticles, the level of the active form of c-Jun decreased to almost that of the control (Figure 7A). Thus, H_2O_2 -induced JNK activation was reduced by higher doses of $C_{60}(C(COOH)_2)_2$. The results indicate that $C_{60}(C(COOH)_2)_2$ nanoparticles exert their effect through the JNK pathway. To our knowledge, although several studies have described that antioxidants diminish cell injury by inactivating the oxidative stress transduction pathway,³⁷ this is the first report to show that antioxidative nanoparticles inhibit H_2O_2 -induced JNK activation.

In addition, previous studies on cell apoptosis caused by JNK activation suggest that JNK participates in a mitochondrial-dependent apoptosis process. Activation of mitochondrial Bax by the JNK pathway induces the release of cytochrome c (cyt c) into the cytosol and ensuing caspase activation and cell death.³⁸ These investigations point out that caspase-3 plays a major role in apoptosis by cleaving several essential cellular proteins such as poly (ADP-ribose), polymerase-1 (PARP), and D4-GDI. Cyt c released from mitochondria into the cytoplasm will trigger caspase activation and thus the so-called mitochondrial or intrinsic apopto-

sis pathway.³⁹ Therefore, to evaluate possible modulation of the mitochondrial apoptotic pathway by $C_{60}(C(COOH)_2)_2$, we assessed several related proteins, that is, cytosolic cyt c, caspase-3, and its target transcriptional protein PARP (Millipore Co.) by use of Western blotting. Results obtained supported our hypothesis

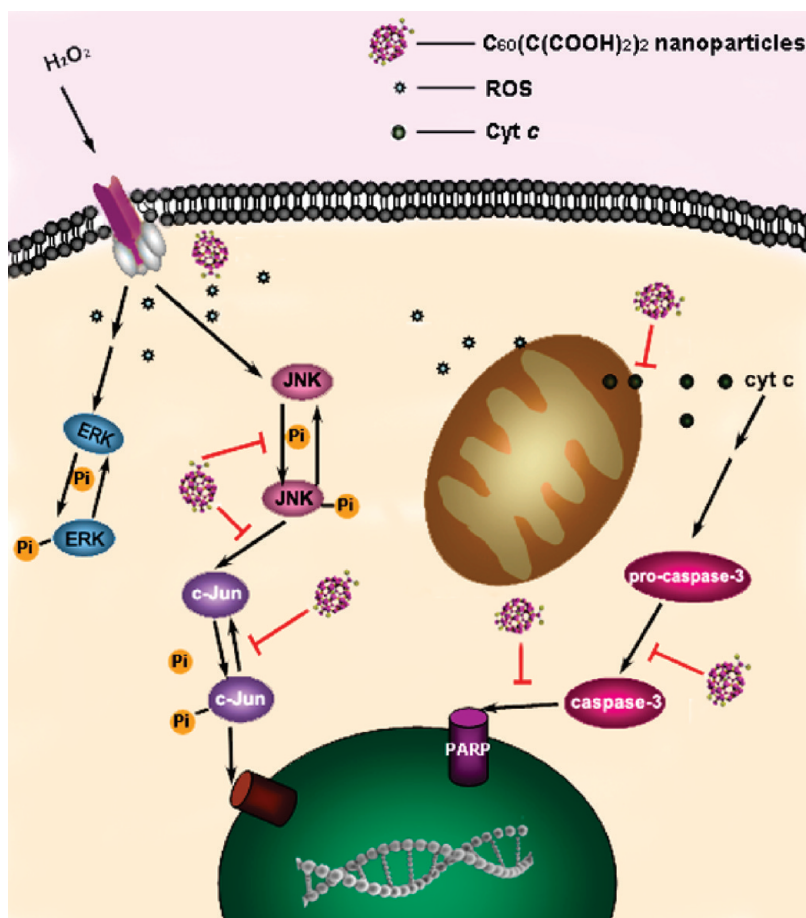


Figure 8. Schematic of the alterations and events in CMECs induced by H_2O_2 and $C_{60}(C(COOH)_2)_2$ treatment. These changes are probably mediated by decreased phosphorylation of JNK and inhibition of ROS production. Consequently, $C_{60}(C(COOH)_2)_2$ treatment can regulate several downstream signaling events, including reduced activation of c-Jun and caspase-3 and inhibition of PARP cleavage and mitochondrial cyt c release.

that inhibit activation of the JNK pathway and c-Jun phosphorylation by showing that incubation with $C_{60}(C(COOH)_2)_2$ significantly decreased apoptotic activation induced by H_2O_2 , inhibited cytosolic cyt *c* release, reduced the activation of caspase-3, and impaired PARP cleavage (Figure 7B). These results confirm that, when $C_{60}(C(COOH)_2)_2$ is present, caspase-dependent apoptosis induced by oxidative stress can be effectively inhibited.

In brief, H_2O_2 triggers JNK activation, induces loss of the mitochondrial membrane potential and cyt *c* release, and hence induces caspase-3 activation which leads to PARP cleavage from the full-length (116 kDa) to 89-kDa form, and finally apoptosis occurs. Our results provide a reasonable and logical explanation for the mechanism underlying increased survival signaling by the administration of $C_{60}(C(COOH)_2)_2$: the active forms of JNK-MAPK-associated mitochondrial dysfunction, caspase-3, and PARP, which constitute the basis for JNK-MAPK-induced apoptosis induced by oxidative stress, can be impaired sequentially by $C_{60}(C(COOH)_2)_2$ thus reducing their capacity to induce apoptosis (Figure 8).

CONCLUSIONS

In summary, on the basis of present results, we have proposed a novel protective scenario in which $C_{60}(C(COOH)_2)_2$ nanoparticles are “recognized” by

oxidation-damaged endothelial cells and are translocated into these abnormal cells. Thereafter, intracellular $C_{60}(C(COOH)_2)_2$ fight against oxidative damage by removing dissociative ROS, and inactivating JNK-related cytoplasmic signaling events that regulate cell apoptosis. Under normal physiological conditions, intact CMECs are not adversely affected by nanoparticles. Herein for the first time a comparison of the potential role of $C_{60}(C(COOH)_2)_2$ in the *in vitro* endothelial cell model from the BBB under pathological and physiological conditions has been made. It is notable, however, that nanoparticles probably do not act directly on signaling proteins, the impaired apoptotic signal might be attributed to $C_{60}(C(COOH)_2)_2$ -neutralization of intracellular ROS. Nevertheless, the underlying mechanism how free radical scavenging functions of $C_{60}(C(COOH)_2)_2$ are integrated during the CMECs response to oxidant and further how $C_{60}(C(COOH)_2)_2$ go through their metabolism and biodegradation within the cells and even the body still require further investigation. Blood brain barrier composed of CMECs serves as a physiological protective shield between the brain microenvironment and circulating blood, where the protective activity of $C_{60}(C(COOH)_2)_2$ may be beneficial for the treatment in BBB relevant disorders. Many challenges and opportunities remain for developing fullerene derivatives with potent biomedical applications.

EXPERIMENTAL METHODS

Preparation of Water-Soluble Fullerene Nanoparticles. $C_{60}(C(COOH)_2)_2$ was produced as described.^{19,20} Six major products of malonate derivatives of C_{60} were obtained from the eluate collected at different retention times by chromatography on silica gel (400 mesh) using different mobile phases, in order of toluene, toluene-hexane (1:1), and hexane. We performed fine separation of the products with HPLC techniques, followed by characterization with MADLI-TOF-MS. The fraction VI of $C_{60}(C(COOH)_2)_2$ (structure as indicated in Figure 1A) was chosen to study the biological effects in the following experiments.

Animals. Male Wistar rats were obtained from the Charles River Laboratories (USA), Beijing Vital River Laboratory Animal Co., Ltd. The animals were housed in a specific pathogen-facility (SPF) according to standard laboratory procedures.

Isolation and Culture of Microvessel Endothelial Cells. Rat CMECs were isolated using a modified method as described previously.⁴⁰ In brief, four immature rats weighing 80–90 g were sacrificed by cervical dislocation, followed by forebrain isolation. Gray matter was homogenized and digested with type II collagenase. After repeated cycles of washing and centrifugation, microvessel pellets were collected and resuspended in 8 mL of Dulbecco's modified Eagle's medium (DMEM), supplemented with 20% fetal bovine serum (FBS) and 7.5 $\mu\text{mol/L}$ endothelial cell growth factor (bECGF, Roche Diagnostics). The purity of endothelial cells was evaluated by the spindle-shaped appearance of cells under phase microscopy and by specific staining of the von Willebrand factor (vWf) as previously described.⁴¹ For preparation of BBB monolayers *in vitro*, CMECs were plated on gelatin-coated 35-mm Petri dishes until they became confluent and formed tight junctions. Rat CMECs from the third passage were used in all experiments. Experiments were repeated at least three times independently and showed similar results.

Antibodies and Reagents. Anti-PARP and anticaspase-3 antibodies were purchased from Millipore Corporation (USA), and anti-

p-JNK and anti-JNK antibodies were purchased from BD Biosciences. Primer pairs for iNos, eNos, and ET-1 were synthesized by Invitrogen, and endothelin-1 (ET-1) radioimmunoassay kits were purchased from Dongya Radioimmuno Inc., China. Griess reagent kits used for the detection of nitric oxide release were purchased from Promega Corporation (USA). Other chemicals and cell culture reagents were purchased from Sigma-Aldrich and HyClone Corporation, respectively, unless otherwise stated.

Cell Viability Assays. Cell viability assays were performed using a Cell Counting-8 Kit (Dojindo Laboratories, Japan) according to the manufacturer's instructions. Cell viability was expressed as the percentage of viable cells in total cell counts. Rat CMECs (1×10^5) were plated as 4-well replicates in a 96-well culture plate (Corning, Inc.). CMECs were incubated with increasing $C_{60}(C(COOH)_2)_2$ nanoparticle doses (1, 10, 25, 50, 100 μM) for 12, 24, 48, and 72 h. To determine the protective half maximal effective concentration (ED_{50}) of nanoparticles against H_2O_2 -induced damage, CMECs were exposed to 300 μM H_2O_2 for 2 h, the media was removed, and the CMECs were washed with PBS three times, followed by incubation with different doses of $C_{60}(C(COOH)_2)_2$ nanoparticles for 24 h. Then the cells were washed with PBS three times before the test.

Observation of Membrane Ultrastructural Morphology with Atom Force Microscopy (AFM) and Environmental Scanning Electronic Microscopy (ESEM). CMECs were seeded onto Petri dishes and cultured until 90% confluence, followed by incubation in the presence or absence of H_2O_2 at a final concentration of 300 μM for 2 h. After being washed with PBS three times to wipe off the H_2O_2 in the media, CMECs were treated with or without 50 μM $C_{60}(C(COOH)_2)_2$ nanoparticles for 24 h, followed by washing three times to remove nonspecific-binding $C_{60}(C(COOH)_2)_2$ nanoparticles. The cells were fixed with 2.5% (v/v) glutaraldehyde and prepared for AFM as described.²⁵ The surface structure of CMECs were observed with a biological AFM (Agilent 5500 Agilent Co.) using the tapping mode in air. Surface areas (10 μm) were randomly selected for scanning by the instrument, and at least four areas were scanned

for each treatment. Data were collected using a scanning rate of 1.0–1.5 Hz, and image analysis was performed with software provided with the imaging module (PicoScan 5.0, USA). For ESEM observation, CMECs were prepared as in the AFM experiment, then were fixed in 2.5% glutaraldehyde for 24 h, dehydrated with series-grade ethanol, and critical-point dried in CO₂. Finally cells were scanned with an environmental scanning electronic microscope (ESEM) (Quanta 200 FEG, FEI Co.). At least four areas for each treatment were randomly scanned for analysis.

Observation of Nanoparticle Translocation. For confocal observation, FITC-labeled C₆₀(C(COOH)₂)₂ nanoparticles were prepared and characterized as described in previous literatures.²⁰ CMECs were incubated in the presence or absence of 300 μM H₂O₂ for 2 h, and washed with PBS three times to remove the H₂O₂ in the media. After CMECs were treated with or without 50 μM FITC-labeled C₆₀(C(COOH)₂)₂ nanoparticles for 24 h, cells were washed three times with PBS before scanning with a confocal laser scanning microscope (CLSM, Olympus FV 500). For transmission electron microscope (TEM, Hitachi H-600, Japan) observation, 10⁶ CMECs were treated in the presence or absence of 300 μM H₂O₂ for 2 h, then the media was removed and cells were washed with PBS before the addition of C₆₀(C(COOH)₂)₂ nanoparticles. After incubation for 24 h the cells were washed with PBS and collected by centrifugation. They were finally fixed in 2.5% glutaraldehyde and prepared for TEM experiments.

Flow Cytometry. Fluorescence double staining with Annexin V-FITC and PI (BD Biosciences) was used and was followed by flow cytometry (FCM, Beckman Coulter Limited Co.). The effect of C₆₀(C(COOH)₂)₂ nanoparticles on intercellular ROS of rat CMECs was assessed further by using a ROS fluorescent probe, 2',7'-dichlorofluorescein diacetate (DCFH-DA). In brief, cultures treated with 300 μM H₂O₂ to induce oxidative stress were washed three times with PBS, followed by incubation with an appropriate dose of fullerene nanoparticles (50, 100 μM) for 24 h. In experiments to study apoptosis, 5 μM Annexin V-FITC and PI were added in cells suspended and washed with PBS three times. The results are plotted on a dot-plot: viable control cells (FITC⁻/PI⁻), apoptotic cells (FITC⁺/PI⁻), and secondary necrotic cells (FITC⁺/PI⁺). To detect ROS generation, 10⁶ cells were loaded with 10 μM DCFH-DA for 15 min before pelleting at 37 °C in the dark. The fluorescence of ROS was detected using confocal microscopy and conventional flow cytometry, and the data was analyzed using WinMDI software.

Actin Fluorescent Staining. CMECs were grown to confluence on glass coverslips, stimulated with 300 μM H₂O₂ for 2 h followed by a PBS wash, and were incubated with vehicle or 50 μM C₆₀(C(COOH)₂)₂ nanoparticles for 24 h. The cells were washed three times with PBS, fixed in freshly prepared 4.0% paraformaldehyde in PBS for 15 min, washed with PBS three times, and permeabilized with 1% Triton X-100 in PBS, pH 7.4 for 5 min. Actin was visualized by rhodamine-labeled phalloidin (1 μM in PBS, with 0.1% BSA) and placed onto the coverslips for 30 min. To visualize nuclei, DNA was stained with the chromatin dye Hoechst 333342 (0.01 M in PBS and 0.1% BSA) for 1 min. Coverslips were washed three times in PBS (0.1% BSA), and cells were viewed under a laser confocal scanning microscope (Olympus FV 500).

Western Blotting. CMECs were cultured in 6-well plate at 10⁶ cell/well and incubated at 37° until 90% confluence. Then cells were stimulated with 300 μM H₂O₂ for 2 h, followed by washed with PBS, and were incubated with vehicle or C₆₀(C(COOH)₂)₂ nanoparticles (50, 100 μM for 24 h). After being washed three times with PBS, the cells were collected and extracted for electrophoresis. For analysis of the expression of particular proteins, PVDF membranes were incubated with anti-caspase-3, anti-JNK, anti-p-JNK, anti-c-Jun, or anti-PARP.

Statistical Analysis. Data (mean ± SEM) were analyzed for normal distribution (one-way or repeated measures ANOVA). The number of single experiments compiled is indicated by *n*. *P* < 0.05 was considered to be a significant difference.

Acknowledgment. This work is financially supported by the Ministry of Science and Technology of China (Grant Nos. 2006CB705603 and 2010CB934004), the Natural Science Foundation of China (NSFC) (Grant Nos. 10525524, 10672192, 90709054

and 10975040), and the CAS Knowledge Innovation Program (KJCX2-YW-M02).

Supporting Information Available: Size distribution of C₆₀(C(COOH)₂)₂; co-localization of C₆₀(C(COOH)₂)₂ and lysosomes; cytotoxicity of C₆₀(C(COOH)₂)₂ and effects on CMEC vaso-relaxing/constrictive functions under normal condition have been shown in Figures S1–S3. This material is available free of charge via the Internet at <http://pubs.acs.org>.

REFERENCES AND NOTES

- Medina, C.; Santos-Martinez, M. J.; Radomski, A.; Corrigan, O. I.; Radomski, M. W. Nanoparticles: Pharmacological and Toxicological Significance. *Br. J. Pharmacol.* **2007**, *150*, 552–558.
- Sengupta, S.; Sasisekharan, R. Exploiting Nanotechnology to Target Cancer. *Br. J. Cancer* **2007**, *96*, 1315–1319.
- Silva, G. A. What Impact Will Nanotechnology Have on Neurology. *Nat. Clin. Pract. Neurol.* **2007**, *3*, 180–181.
- Hong, B.; Kai, J.; Ren, Y.; Han, J.; Zou, Z.; Ahn, C. H.; Kang, K. A. Highly Sensitive, Rapid, Reliable, and Automatic Cardiovascular Disease Diagnosis with Nanoparticle Fluorescence Enhancer and Membr. *Adv. Exp. Med. Biol.* **2008**, *614*, 265–73.
- Kontos, H. A. Oxygen Radicals in Cerebral Vascular Injury. *Circ. Res.* **1985**, *57*, 508–516.
- Chan, P. H. Oxygen Radicals in Focal Cerebral Ischemia. *Brain Pathol.* **1994**, *4*, 59–65.
- Oldendorf, W. H.; Cornford, M. E.; Brown, W. J. The Large Apparent Work Capability of the Blood-Brain Barrier: A Study of the Mitochondrial Content of Capillary Endothelial Cells in Brain and Other Tissues of the Rat. *Ann. Neurol.* **1977**, *1*, 409–417.
- Lee, H. S.; Namkoong, K.; Kim, D. H.; Kim, K. J.; Cheong, Y. H.; Kim, S. S.; Lee, W. B.; Kim, K. Y. Hydrogen Peroxide-Induced Alterations of Tight Junction Proteins in Bovine Brain Microvascular Endothelial Cells. *Microvasc. Res.* **2004**, *68*, 231–238.
- Huang, J.; Agus, D. B.; Winfree, C. J.; Kiss, S.; Mack, W. J.; McTaggart, R. A.; Choudhri, T. F.; Kim, L. J.; Mocco, J.; Pinsky, D. J.; et al. Dehydroascorbic Acid, a Blood-Brain Barrier Transportable Form of Vitamin C, Mediates Potent Cerebroprotection in Experimental Stroke. *Proc. Natl. Acad. Sci. U.S.A.* **2001**, *98*, 11720–117204.
- McCarron, R. M.; Shohami, E.; Panikashvili, D.; Chen, Y.; Golech, S.; Strasser, A.; Mechoulam, R.; Spatz, M. Antioxidant Properties of the Vasoactive Endocannabinoid, 2-Arachidonoyl Glycerol (2-AG). *Acta Neurochir. Suppl.* **2003**, *86*, 271–275.
- Peden, D. B.; Hohman, R.; Brown, M. E.; Mason, R. T.; Berkebile, C.; Fales, H. M.; Kaliner, M. A. Uric Acid Is a Major Antioxidant in Human Nasal Airway Secretions. *Proc. Natl. Acad. Sci. U.S.A.* **1990**, *87*, 7638–7642.
- Niu, J.; Azfer, A.; Rogers, L. M.; Wang, X.; Kolattukudy, P. E. Cardioprotective Effects of Cerium Oxide Nanoparticles in a Transgenic Murine Model of Cardiomyopathy. *Cardiovasc. Res.* **2007**, *73*, 549–559.
- Olivier, J. C. Drug Transport to Brain with Targeted Nanoparticles. *NeuroRx* **2005**, *2*, 108–119.
- Ali, S. S.; Hardt, J. I.; Quick, K. L.; Kim-Han, J. S.; Erlanger, B. F.; Huang, T. T.; Epstein, C. J.; Dugan, L. L. A Biologically Effective Fullerene (C₆₀) Derivative with Superoxide Dismutase Mimetic Properties. *Free Radic. Biol. Med.* **2004**, *37*, 1191–1202.
- Dugan, L. L.; Turetsky, D. M.; Du, C.; Lobner, D.; Wheeler, M.; Almlı, C. R.; Shen, C. K.; Luh, T. Y.; Choi, D. W.; Lin, T. S. Carboxyfullerenes as Neuroprotective Agents. *Proc. Natl. Acad. Sci. U.S.A.* **1997**, *94*, 9434–9439.
- Bisaglia, M.; Natalini, B.; Pellicciari, R.; Straface, E.; Malorni, W.; Monti, D.; Franceschi, C.; Schettini, G. C3-Fullero-tris-methanodicarboxylic Acid Protects Cerebellar Granule Cells from Apoptosis. *J. Neurochem.* **2000**, *74*, 1197–1204.

17. Lin, A. M.; Chyi, B. Y.; Wang, S. D.; Yu, H. H.; Kanakamma, P. P.; Luh, T. Y.; Chou, C. K.; Ho, L. T. Carboxyfullerene Prevents Iron-Induced Oxidative Stress in Rat Brain. *J. Neurochem.* **1999**, *72*, 1634–1640.
18. Dugan, L. L.; Lovett, E. G.; Quick, K. L.; Lotharius, J.; Lin, T. T.; O'Malley, K. L. Fullerene-Based Antioxidants and Neurodegenerative Disorders. *Parkinsonism Relat. Disord.* **2001**, *7*, 243–246.
19. Hirsch, A.; Lamparth, I.; Karfunkel, H. R. Functionalization of Fullerenes and Carbon Nanotubes. *Angew. Chem., Int. Ed. Engl.* **1994**, *33*, 437–438.
20. Li, W.; Chen, C. Y.; Ye, C.; Wei, T. T.; Zhao, Y. L.; Lao, F.; Chen, Z.; Meng, H.; Gao, Y. X.; Yuan, H.; *et al.* The Translocation of Fullerene Nanoparticles into Lysosome via the Pathway of Clathrin-Mediated Endocytosis. *Nanotechnology.* **2008**, *19*, 145102–145116.
21. Yin, J. J.; Lao, F.; Fu, P. P.; Wamer, W. G.; Zhao, Y.; Wang, P. C.; Liang, X. J.; Chen, C. The Scavenging of Reactive Oxygen Species and the Potential for Cell Protection by Functionalized Fullerene Materials. *Biomaterials* **2009**, *30*, 611–621.
22. Tampo, Y.; Kotamraju, S.; Chitambar, C. R.; Kalivendi, S. V.; Keszler, A.; Joseph, J.; Kalyanaraman, B. Oxidative Stress-Induced Iron Signaling Is Responsible for Peroxide-Dependent Oxidation of Dichlorodihydrofluorescein in Endothelial Cells: Role of Transferrin Receptor-Dependent Iron Uptake in Apoptosis. *Circ. Res.* **2003**, *92*, 56–63.
23. Parat, M. O.; Stachowicz, R. Z.; Fox, P. L. Oxidative Stress Inhibits Caveolin-1 Palmitoylation and Trafficking in Endothelial Cells. *Biochem. J.* **2002**, *361*, 681–688.
24. Koppal, T.; Drake, J.; Yatin, S.; Jordan, B.; Varadarajan, S.; Bettenhausen, L.; Butterfield, D. A. Peroxynitrite-Induced Alterations in Synaptosomal Membrane Proteins: Insight into Oxidative Stress in Alzheimer'S Disease. *J. Neurochem.* **1999**, *72*, 310–317.
25. Pfister, G.; Stroh, C. M.; Perschinka, H.; Kind, M.; Knoflach, M.; Hinterdorfer, P.; Wick, G. Detection of HSP60 on the Membrane Surface of Stressed Human Endothelial Cells by Atomic Force and Confocal Microscopy. *J. Cell. Sci.* **2005**, *118*, 1587–1594.
26. Sangeetha, P.; Balu, M.; HariPriya, D.; Panneerselvam, C. Age Associated Changes in Erythrocyte Membrane Surface Charge: Modulatory Role of Grape Seed Proanthocyanidins. *Exp. Gerontol.* **2005**, *40*, 820–828.
27. Fung, L. W.; Kalaw, B. O.; Hatfield, R. M.; Dias, M. N. Erythrocyte Spectrin Maintains Its Segmental Motions on Oxidation: A Spin-Label EPR Study. *Biophys. J.* **1996**, *70*, 841–851.
28. Wautier, J. L.; Paton, R. C.; Wautier, M. P.; Pintigny, D.; Abadie, E.; Passa, P.; Caen, J. P. Increased Adhesion of Erythrocytes to Endothelial Cells in Diabetes Mellitus and Its Relation to Vascular Complications. *N. Engl. J. Med.* **1981**, *305*, 237–242.
29. Beppu, M.; Hayashi, T.; Hasegawa, T.; Kikugawa, K. Recognition of Sialosaccharide Chains of Glycophorin on Damaged Erythrocytes by Macrophage Scavenger Receptors. *Biochim. Biophys. Acta* **1995**, *1268*, 9–19.
30. Lai, C. H.; Kuo, K. H.; Leo, J. M. Critical Role of Actin in Modulating BBB Permeability. *Brain Res. Brain Res. Rev.* **2005**, *50*, 7–13.
31. Wang, J. X.; Chen, C. Y.; Li, B.; Yu, H. W.; Zhao, Y. L.; Sun, J.; Li, Y.; Xing, G. M.; Yuan, H.; Tang, J.; *et al.* Antioxidative Function and Biodistribution of [Gd@C82(OH)22]n Nanoparticles in Tumor-Bearing Mice. *Biochem. Pharmacol.* **2006**, *71*, 872–881.
32. Davis, R. J. Signal Transduction by the JNK Group of MAP Kinases. *Cell* **2000**, *103*, 239–252.
33. Cuda, G.; Paterno, R.; Ceravolo, R.; Candigliota, M.; Perrotti, N.; Perticone, F.; Faniello, M. C.; Schepis, F.; Ruocco, A.; Mele, E.; *et al.* Protection of Human Endothelial Cells from Oxidative Stress: Role of Ras-ERK1/2 Signaling. *Circulation* **2002**, *105*, 968–974.
34. Johnson, N. L.; Gardner, A. M.; Diener, K. M.; Lange-Carter, C. A.; Gleavy, J.; Jarpe, M. B.; Minden, A.; Karin, M.; Zon, L. I.; Johnson, G. L. Signal Transduction Pathways Regulated by Mitogen-Activated/Extracellular Response Kinase Kinase Kinase Induce Cell Death. *J. Biol. Chem.* **1996**, *271*, 3229–3237.
35. Moreno-Manzano, V.; Ishikawa, Y.; Lucio-Cazana, J.; Kitamura, M. Suppression of Apoptosis by All-trans-Retinoic Acid. Dual Intervention in the c-Jun n-Terminal Kinase-AP-1 Pathway. *J. Biol. Chem.* **1999**, *274*, 20251–20258.
36. Anfuso, C. D.; Lupo, G.; Romeo, L.; Giurdanella, G.; Motta, C.; Pascale, A.; Tirolo, C.; Marchetti, B.; Alberghina, M. Endothelial Cell-Pericyte Cocultures Induce PLA2 Protein Expression through Activation of PKC α and the MAPK/ERK Cascade. *J. Lipid. Res.* **2007**, *48*, 782–793.
37. Lee, S. H.; Heo, J. S.; Lee, M. Y.; Han, H. J. Effect of Dihydrotestosterone on Hydrogen Peroxide-Induced Apoptosis of Mouse Embryonic Stem Cells. *J. Cell. Physiol.* **2008**, *216*, 269–275.
38. Perier, C.; Bove, J.; Wu, D. C.; Dehay, B.; Choi, D. K.; Jackson-Lewis, V.; Rathke-Hartlieb, S.; Bouillet, P.; Strasser, A.; Schulz, J. B.; *et al.* Two Molecular Pathways Initiate Mitochondria-Dependent Dopaminergic Neurodegeneration in Experimental Parkinson's Disease. *Proc. Natl. Acad. Sci. U.S.A.* **2007**, *104*, 8161–8166.
39. Newmeyer, D. D.; Ferguson-Miller, S. Mitochondria: Releasing Power for Life and Unleashing the Machineries of Death. *Cell* **2003**, *112*, 481–490.
40. Folkman, J.; Haudenschield, C. C.; Zetter, B. R. Long-Term Culture of Capillary Endothelial Cells. *Proc. Natl. Acad. Sci. U.S.A.* **1979**, *76*, 5217–5221.
41. Han, D.; Ma, W. Y.; Liao, F. L.; Yeh, M. L.; Ouyang, Z. G.; Sun, Y. X. Time-Series Observation of the Spreading of of Microvessel Endothelial Cells with Atomic Force Microscopy. *Phys. Med. Biol.* **2003**, *48*, 3897–3909.